ELSEVIER

Engineering Structures 22 (2000) 1699–1706

ENGINEERING STRUCTURES

www.elsevier.com/locate/engstruct

Preliminary design of very long-span suspension bridges

Paolo Clemente [a,*], Giulio Nicolosi [b], Aldo Raithel [b]

[a] *ENEA—Centro Ricerche Casaccia, via Anguillarese 301, 00060 S.M. Galeria, Roma, Italy*
[b] *Dipartimento di Analisi e Progettazione Strutturale, Università di Napoli Federico II, via Claudio 21, 80125 Napoli, Italy*

Received 27 January 1999; received in revised form 25 November 1999; accepted 26 November 1999

Abstract

The feasibility of very long-span suspension bridges is analysed. The relation between the geometrical parameters, the load and the material characteristics is first discussed in order to find out the limit value of the span length. An iteration procedure is then proposed to study the main aspects of the structural behaviour in the deflection theory. The results of a numerical investigation allow to state that the behaviour of a very long-span suspension bridge, both in terms of stresses and deflection, is similar to the behaviour of an unstiffened cable, the contribution of the girder being negligible.

Keywords: Suspension bridges; Long-span bridges; Limit span; Deflection theory

1. Introduction

Suspension bridges were already built by primitive man, by using ropes of creepers, anchored to towers of natural rock. The first iron chain bridge appeared perhaps in China [1]. In the eighteenth century, chains of wrought iron were introduced in England and the USA. Most of the chain bridges collapsed because of oscillations due to wind actions. The first wire cable suspension bridges were built at the beginning of the nineteenth century.

In 1883 the 580 m span Brooklyn Bridge was successfully completed. It was considered as the eighth wonder in the world and its success encouraged the engineers to use the suspension bridge for all the new long-span bridges.

Between the last decades of the nineteenth century and the first ones of this century, first the elastic theory and then the deflection theory developed [2]. These advances in the understanding of suspension bridge behaviour affected a great expansion of their use, especially in the USA. The George Washington Bridge of about 1000 m span, opened in 1931, represented a great step forward the construction of long-span bridges. A few years later, in 1937, the Golden Gate Bridge, with a main span on 1240 m, was completed.

The glamorous failure of the Tacoma Narrows Bridge in 1940 caused a stop in the span increasing and major efforts were made in order to understand the behaviour of suspension bridges under wind loads.

In recent years very long-span suspension bridges were designed. The Great Belt East Bridge in Denmark, characterised by a wind transparent deck, shows a 1624 m main span. The Akashi Kaikyo Bridge in Japan has a main span of 1991 m. A suspension bridge of 3300 m has been proposed to span the Messina Strait and finally, a new type with three spans of 5000 m has been analysed for the Gibraltar Strait crossing [3].

The reasons for increased spans are known. First of all the increase of the horizontal navigation clearances, in order to accommodate the increasing size and volume of marine traffic. Then the economic trade off of span length cost of deep water foundations, as opposed to shallow water foundations, and the risk of ship collision with piers.

The feasibility of longer spans is related to the implementation of new high-strength lightweight materials. As a matter of fact, as spans become longer, cables become heavier. Therefore, a high percentage of the cable stress is related to its own self-weight. Furthermore the stiffening contribution of the deck on the structural behaviour becomes negligible.

In the present paper the analysis of the structural

* Corresponding author. Tel.: + 39-06-30486297; fax + 39-06-30484872.
E-mail address: paolo.clemente@casaccia.enea.it (P. Clemente).

0141-0296/00/$ - see front matter
PII: S0141-0296(99)00112-1

behaviour of very long-span suspension bridges is carried out. A very simple relationship between the span, the load and the cable cross-sectional area is discussed, in order to find out the maximum value of the span length. A very rapid iteration procedure is proposed that allows to analyse the behaviour of very long-span suspension bridges in the deflection theory. The results of a large numerical investigation are shown, that point out the influence of the span on stresses and deflection.

2. Limit span

Consider first the case of an unstiffened cable, i.e. a suspension bridge without stiffening girders. This model, which is suitable (a) to perform the preliminary design of the structure and (b) to have a first glance at its displacements, is shown in Fig. 1. We assume the sag ratio f/ℓ in the middle of the main span, and the maximum value α_m of the slope angle α, with respect to the horizontal, to be fixed. So the following non-dimensional geometrical parameter is defined:

$$k = f/\ell \cdot \cos \alpha_m \tag{1}$$

For the usual values of f/ℓ ($\cong 0.10$) we can suppose the total self-weight of the cable to be uniformly distributed on the main span. If A_c is the cable cross-sectional area and γ_c the cable weight per unit volume, then the uniformly distributed self-weight of the cable is

$$w_c = \gamma_c A_c \cdot L_c/\ell = \gamma A_c$$

L_c being the cable length. The ratio L_c/ℓ depends on the cable shape only. So, for a fixed shape, i.e. for a given k, γ is proportional to γ_c. If w_p is the permanent load on the main span, which is also supposed to be uniform, the dead load per unit length can be written:

$$w = w_p + \gamma A_c \tag{2}$$

Two kinds of travelling loads are considered: a uniform load acting on the whole main span

$$p_1 = \beta_1 \cdot w \tag{3}$$

and a uniform load coming to the main span

$$p_2 = \beta_2 \cdot w \tag{4}$$

whose maximum length is $c_2\ell$ ($c_2 < 1$).

The horizontal component of tension in the cable is H_w under dead loads only and H under combined dead and live loads. We conventionally put:

$$H = H_w + H_p \tag{5}$$

H_p as being the increment of tension caused by live loads acting on the structure.

Consider p_{eq} to be the uniform load acting on the whole main span, that causes the same horizontal tension in the cable of the loads p_1 and p_2. If p_2 is symmetric around to the mid-span and starts at a distance of $c_1\ell$ from the left pier, then:

$$p_{eq} = p_1 + p_2 \cdot (1 - 4c_1^2) \tag{6}$$

If we put

$$\beta = (w_p + p_{eq})/\gamma A_c \tag{7}$$

then the value of the horizontal tension and the corresponding maximum value of the axial force in the cable are, respectively:

$$H = \gamma A_c \cdot (1 + \beta)\ell/(8f/\ell) \qquad N_{max} = \gamma A_c \cdot (1 + \beta)\ell/8k \tag{8}$$

The non-dimensional parameter β is the ratio between the additional load, which the cable supports, and its self-weight. If $\beta = 0$, then the cable bears its self-weight only.

By setting N_{max} to the allowable value of the tension in the cable, σA_c , we deduce, for a given β, the limit value of the span, i.e. the maximum value of the span length for a cable of cross-sectional area A_c, compatible with the assigned loads and material strength:

$$\ell_{lim} = 8k \cdot (\sigma/\gamma)/(1 + \beta) \tag{9}$$

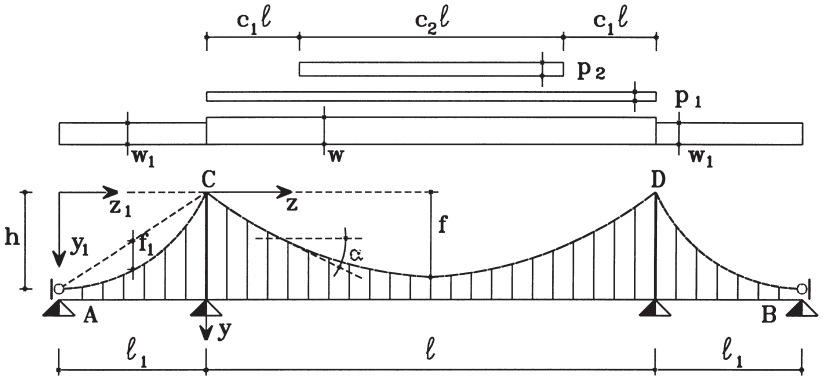

Fig. 1. Unstiffened cable model.

Consider first the limit case of the cable subject to self-weight only ($\beta = 0$). The limit value of the span becomes independent of the cable section and depends only on the characteristics of the material and on the defined geometry of the structure

$$\ell_{0,\lim} = 8k\cdot\sigma/\gamma \tag{10}$$

If live loads are acting on the structure ($\beta > 0$), then the limit value of the span depends also on the value of the live loads and on the cable cross-sectional area, that determine the value of β. Eq. (9) can be used for the preliminary design of the cable, by solving it for A_c:

$$A_c = \frac{(w_p + p_{eq})}{8k\sigma/\ell - \gamma} \tag{11}$$

Eq. (11) is meaningful only for $\ell < \ell_{0,\lim}$. In fact, $A_c \to \infty$ when $\ell \to \ell_{0,\lim}$.

In Fig. 2 the diagram of the non-dimensional parameter $\ell_{\lim}/(k\sigma/\gamma)$ versus β is plotted. As one can see $\ell_{\lim}$ decreases rapidly when β increases. For the usual case of $k = 0.1$, and considering a steel cable for which $\sigma/\gamma \cong 10^4$ m, the diagram in Fig. 2 gives the limit span value in km. High values of the sag ratio determine lower stresses in the cable and so allow to span larger distances, but the cost of the piers becomes prohibitive. In the case of materials characterised by higher values of the ratio σ/γ, the theoretical limit span grows remarkably.

Fig. 2 can also used in a different way. It produces, for a fixed ℓ, the maximum value of β, i.e. the maximum load increment, as a percentage of the self-weight, which the cable can support.

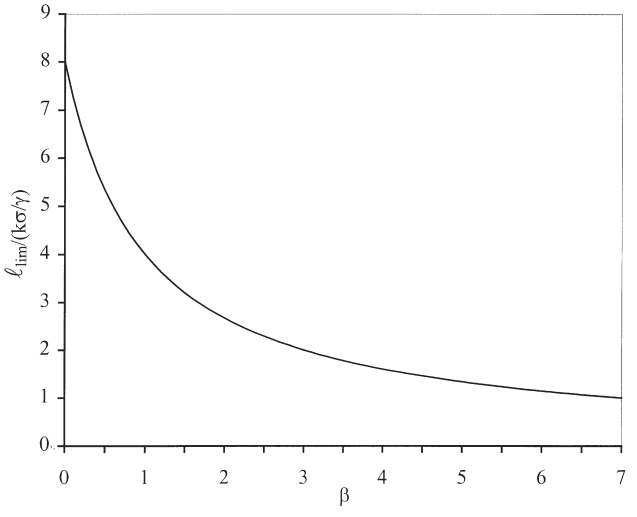

Fig. 2. $\ell_{\lim}/(k\sigma/\gamma)$ against β.

3. Iteration procedure for the non-linear analysis of suspension bridges

Under dead loads only, the co-ordinates of the cable are z and y (z_1 and y_1 in the side span—see Fig. 1). When a generic live load $p(z)$ is acting, the system shows the vertical displacement $v(z)$, which must satisfy the equilibrium equation (see Appendix A)

$$EI\cdot v^{IV}(z) - H\cdot v''(z) = p(z) - wH_p/H_w \tag{12}$$

and the compatibility condition relative to the cable length. The solution can be found by using an iterative procedure [4].

Alternatively, in order to determine the horizontal component of cable tension H, the procedure proposed by Franciosi [5] can be used, that rapidly leads to the same results. It is based on the consideration that, in the same approximation of the deflection theory, in a structure subject to a fixed axial force system, the principle of the superposition of the effects, and so the theorems of the theory of elasticity based on it, are still valid referring to the transversal loads. In a suspension bridge the axial force system is made up by w and H_w, whereas the live loads represent the transversal ones.

In order to apply the Betti theorem, consider the systems of Fig. 3(a) and (b). The model of Fig. 3(a) is the actual structure, subject to dead loads w (w_1 on the side span), to live load $p(z)$ and to temperature variation $\pm \Delta T$, in which the horizontal constraints at the ends have been substituted by the horizontal component of the reaction $H_w + H_p$. The model of Fig. 3(b) (auxiliary system) is the same as the structure of Fig. 3(a) subject to load w and to the horizontal forces $H_w + H_p$ at the ends. It shows the vertical displacements $\eta(z)$ and the relative horizontal displacement δ between the two ends. The Betti theorem enables us to write

$$\int p\eta(z)\cdot dz + H_p\delta = -\int \frac{H_p}{\cos\alpha}\omega\Delta T ds \tag{13}$$

Where ω is the thermal expansion coefficient of the cable material. It is:

$$H_p = -\frac{\int p\eta\cdot dz}{\delta + \int \frac{\omega\Delta T}{\cos\alpha} ds} \tag{14}$$

From Eq. (14) we can determine the increment of the horizontal component of the cable tension due to live load, when $\eta(z)$ and δ are established. If X is the bending moment in the stiffening girder at sections C and D of the system in Fig. 3(b), and we put $a^2 = H/EI$ ($a_1^2 = H/EI_1$), $\eta(z)$ and δ are produced by the following relations:

$$\eta(z) = Ce^{az} + De^{-az} - \frac{H_p}{H}y + \frac{X}{H\ell}z - \frac{H_p}{Ha^2}y''$$

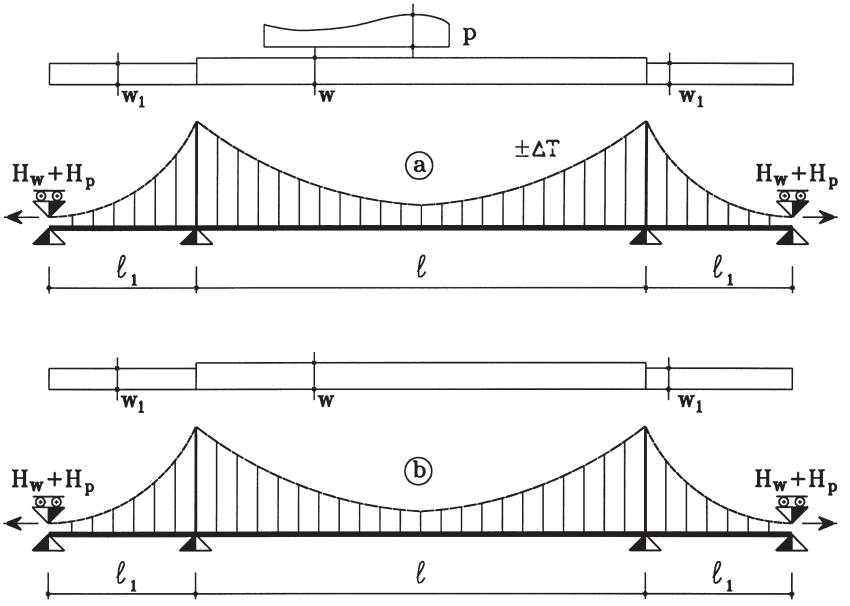

Fig. 3. Actual (a) and auxiliary (b) systems.

$$\eta_1(z_1) = C_1 e^{a_1 z_1} + D_1 e^{-a_1 z_1} - \frac{H_p}{H}\bar{y_1} + \frac{X}{H\ell_1}z_1 \qquad (15)$$

$$- \frac{H_p}{Ha_1^2}y_1''$$

in the main and side spans respectively, and

$$\delta = \frac{H_a}{EA}L_s + 2\frac{H}{EI_1}\int_0^{\ell_1}\bar{y_1}\eta_1 dz + \frac{H}{EI}\int_0^{\ell} y\eta dz \qquad (16)$$

$$+ \frac{16}{15}\left(\frac{f_1^2\ell_1}{EI_1} + \frac{f^2\ell}{2EI}\right)H_p - \frac{2}{3}\left[\frac{f_1\ell_1}{EI_1} + \frac{f\ell}{EI}\right]X$$

in which h is the height of the pylon (see Fig. 1) and

$$\bar{y_1} = y_1 - (\ell_1 - z_1)\cdot h/\ell_1 \qquad (17)$$

In Appendix A, how to achieve at Eqs. (15) and (16) and also how to determine X is explained. The expressions of constants C, D, C_1, D_1 and L_s are also given in Appendix A.

Eqs. (14)–(16) can be solved using an iterative procedure. This can be started by assigning a value of H, calculating X (see Appendix A) and then $\eta(z)$ and δ from Eqs. (15) and (16). Then Eq. (14) produces a new value of H and so on. The solution is found with a few iterations.

If H is known, the equilibrium configuration can be determined from Eq. (12), whose solution has been found, in the following numerical investigation, by using a finite differences procedure.

4. Stresses and deflections in very long-span suspension bridges

A numerical investigation has been carried out by using the previously described procedure. The analysed model is shown in Fig. 4. The main span has been supposed to be simply supported at C and D ($X = 0$). The influence of ℓ on the structural behaviour has been pointed out, in particular. This study being referred to future bridges, values of ℓ from 1000 to 3500 m have been considered, with $f/\ell = 0.10$.

The analysis has been carried out by referring to realistic values of the loads. The permanent load w_1, i.e., the summation of the weight of the deck and the weight of the suspension elements, has been assumed equal to 250 kN/m. The uniform load p_1 acting on the whole middle span is equal to 20 kN/m. A uniform load p_2 = 300 kN/m, coming to the bridge and whose maximum length is 750 m, has also been considered. Load p_1 represents a slight vehicular load, p_2 both heavy vehicular and railway loads. The cable cross-sectional area has been calculated by using Eq. (11), in which σ = 850 MPa and $\gamma = 0.078$ MN/m^3 have been assumed, these being the typical values for steel cables.

In Fig. 5 the diagram of the ratio p/w against the span ℓ is plotted, p being the total live load distributed on the whole main span: $p = (p_1 + p_2\ c_2)$. It is apparent that, because of the increase of w, this ratio becomes very low as ℓ gets higher. It is $p/w = 0$ for $\ell = \ell_{0,\lim}$.

The maximum value H_{max} of the horizontal component of the cable tension occurs when p_2 is placed symmetrically around mid-span. For this load condition the

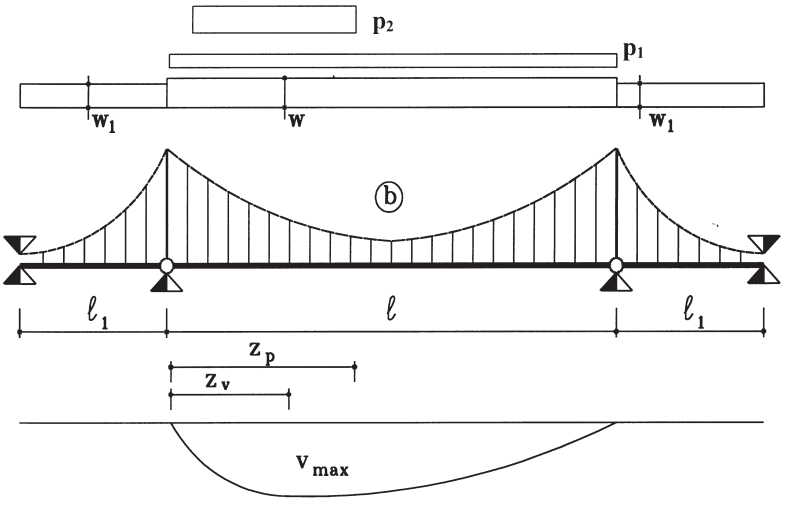

Fig. 4. Investigated model.

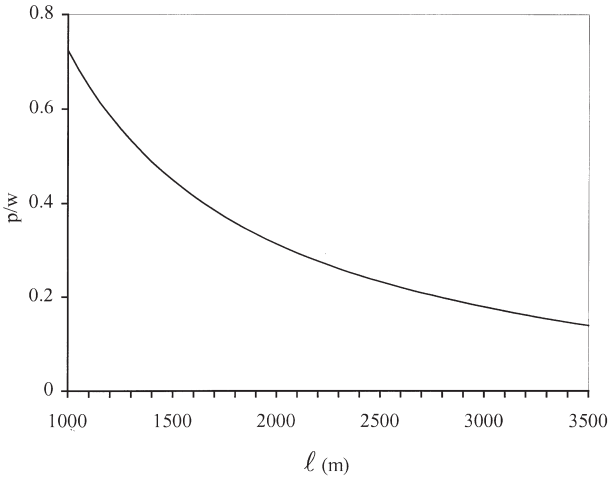

Fig. 5. p/w against ℓ.

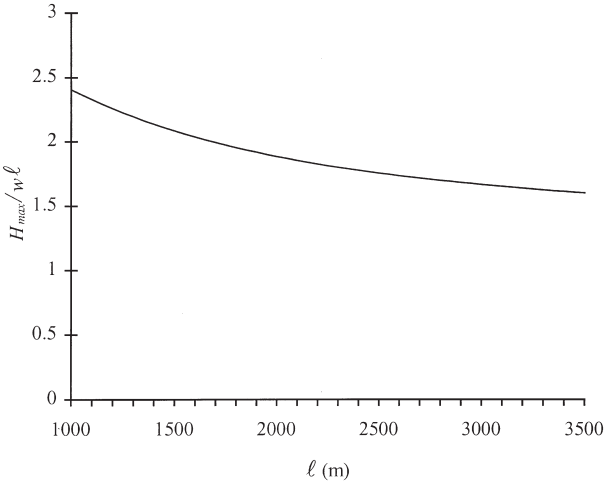

Fig. 6. $H_{max}/w\ell$ against ℓ.

diagram of the non-dimensional ratio $H_{max}/w\ell$ against ℓ is shown in Fig. 6. It diminishes as ℓ gets higher and tends to a limit value related to the ratio f/ℓ.

In Fig. 7 the diagrams of the non-dimensional maximum displacement v/ℓ against ℓ, for different values of the girder bending stiffness EI [MN.m^2], are plotted. The Young's modulus E_c = 180 000 MPa has been assumed for the cable. If $EI = 0$, then v/ℓ gets lower as ℓ increases. This behaviour is due to the increase of w. In fact, $w \to \infty$ when $\ell \to \ell_{0,lim}$. A slope variation is apparent in the curve; the value of ℓ for which this occurs is obviously related to the length of load p_2 (750 m). The curves relative to different values of EI show that the influence of the girder bending stiffness is negligible for high values of ℓ. For ℓ = 3500 m, it is v/ℓ = 0.005. As ℓ gets shorter the contribution of EI becomes stronger so that a reduction of v/ℓ can be observed when ℓ decreases. The value of ℓ for which v/ℓ is maximum is related to the length of the load p_2. This behaviour confirms that for a normal span a noticeable reduction of the displacement is obtained if the girder bending stiffness is high.

The section in which the maximum displacement occurs and the relative position of the moving load p_2 are shown in Fig. 8. In more detail, the non-dimensional abscissa z_v/ℓ of the section in which the maximum displacement v occurs and the relative abscissa of the head of the coming load z_p/ℓ are plotted. The first is practically independent of the span ℓ and equal to 0.27. The second varies in a wider range. In both the diagrams a variation in the slope is evident at $\ell \cong 1500$ m, related to the length of the load p_2 (750 m). The diagram of the ratio $H/w\ell$ for the same load condition is plotted in Fig. 9, in which the previously pointed out singularity can also be observed.

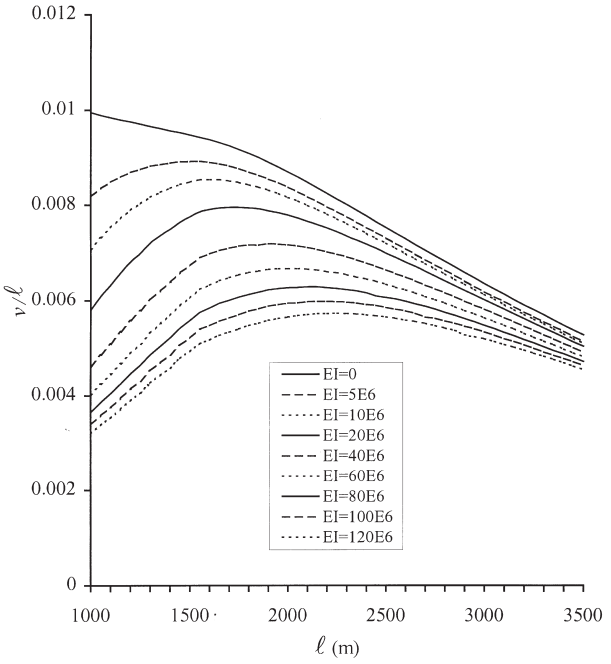

Fig. 7. Non-dimensional maximum displacement v/ℓ against ℓ.

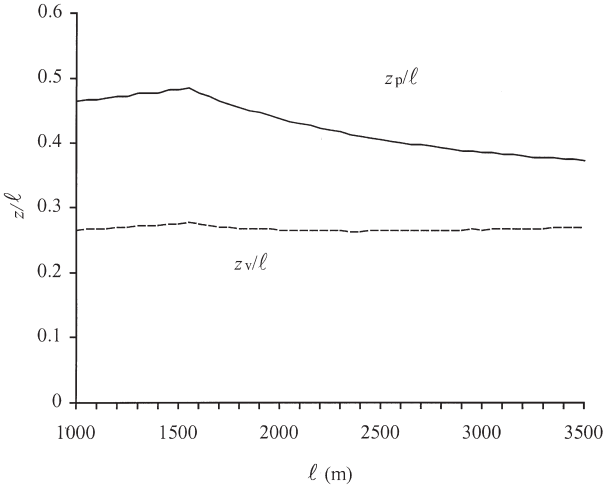

Fig. 8. z_v/ℓ and z_p/ℓ against ℓ.

5. Conclusions

The structural analysis has been performed using an iteration procedure in the same approximation of the deflection theory. The numerical investigation, carried out by means of a specific computer code, allowed to check the fast convergence of the procedure. The main aspects of the structural behaviour have been analysed both in terms of stresses and deflections considering real loading. The result can be summarised as follows:

- The behaviour of a suspension bridge when the span increases, tends to the behaviour of an unstiffened cable and the contribution of the girder becomes negligible;

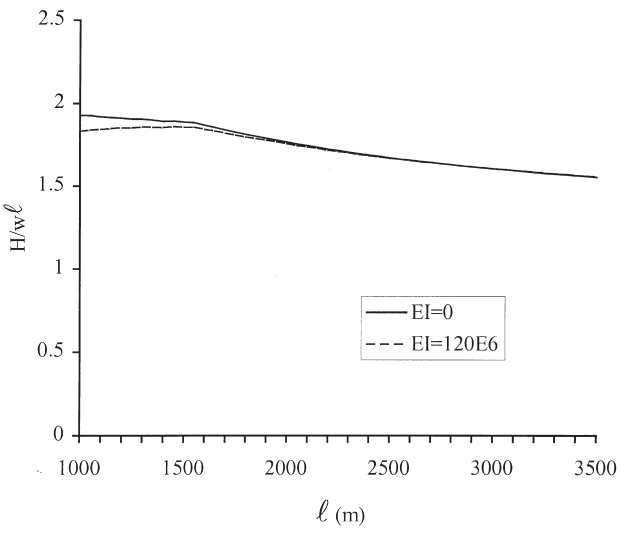

Fig. 9. $H/w\ell$ against ℓ.

- The deformability, in terms of non-dimensional maximum displacement v/ℓ, becomes independent of the girder bending stiffness and decreases when ℓ increases;
- The load condition, which gives the maximum displacement, individualised by the head of the load p_2, z_v/ℓ, and the section in which the maximum displacement occurs, whose non-dimensional abscissa is z_L/ℓ, are independent of the span ℓ.

A very simple relationship between the span, the load and the cable cross-sectional area has also been discussed. It has been deduced considering vertical static loads only and referring to a linear analysis. The nonlinear analysis under static load gives longer values of the limit span, but the analysis in presence of wind loading determines a reduction of the real limit span.

Obviously, the limit span of a suspension bridge is also related to the material characteristics. New materials, characterised by high values of the ratio σ/γ seem to allow to span very long distances in the future, but in this case the effects of wind loading are much higher. The use of new structural types is advisable in order to span longer distances in the future [6].

Appendix A

A.1. Equilibrium equation

The bending moment M in the generic section is

$$M(z) = M_0(z) - (H_w + H_p)\cdot(y(z) + v(z))$$

where M_0 is the bending moment in a simply supported beam of the same span and subject to the same load. The second derivative of the previous expression gives:

$$-EI\cdot v^{IV}(z) = -(w + p(z)) - (H_w + H_p)\cdot y''(z) - (H_w + H_p)\cdot v''(z)$$

And keeping into account that $H_w\cdot y''(z) = -w$, we obtain finally:

$$EI\cdot v^{IV}(z) - H\cdot v''(z) = p(z) - wH_p/H_w$$

A.2. Determination of η and δ

In order to calculate the displacements $\eta(z)$ [Fig. 3(b)], consider the equilibrium equation in the main span:

$$-H\eta - H_p y + X = -EI\eta''$$

where X is the bending moment at sections C and D, E and I the Young's modulus and the moment of inertia of the girder respectively. By putting

$$a^2 = H/EI$$

the previous equation can be written in the form

$$\eta'' - a^2\eta = \frac{H_p}{EI}y - \frac{X}{EI}$$

The complete solution, sum of the complementary and particular solutions, is

$$\eta(z) = Ce^{az} + De^{-az} - \frac{H_p}{H}y + \frac{X}{H} - \frac{H_p}{Ha^2}y''$$

where:

$$y'' = -8f/\ell^2$$

With the boundary conditions

$$\eta(0) = 0 \quad \eta(\ell) = 0$$

the constants C and D are:

$$C = -\frac{H_p}{H}\cdot\frac{8f}{a^2\ell^2}\cdot\frac{1 - e^{-a\ell}}{e^{a\ell} - e^{-a\ell}} - \frac{1 - e^{-a\ell}}{e^{a\ell} - e^{-a\ell}}\cdot\frac{X}{H}$$

$$D = -\frac{H_p}{H}\cdot\frac{8f}{a^2\ell^2}\cdot\frac{e^{a\ell} - 1}{e^{a\ell} - e^{-a\ell}} - \frac{e^{a\ell} - 1}{e^{a\ell} - e^{-a\ell}}\cdot\frac{X}{H}$$

For the side span we obtain, analogously:

$$\eta_1'' - a_1^2\eta_1 = \frac{H_p}{EI_1}\bar{y_1} - \frac{X}{EI_1}\frac{z_1}{\ell_1}$$

in which

$$\bar{y_1} = y_1 - (\ell_1 - z_1)\cdot h/\ell_1$$

The complete solution is:

$$\eta_1(z_1) = C_1e^{a_1z_1} + D_1e^{-a_1z_1} - \frac{H_p}{H}\bar{y_1} + \frac{X}{H\ell_1}z_1 - \frac{H_p}{Ha_1^2}y_1''$$

in which

$$C_1 = -\frac{H_p}{H}\cdot\frac{8f_1}{a_1^2\ell_1^2}\cdot\frac{1 - e^{-a_1\ell_1}}{e^{a_1\ell_1} - e^{-a_1\ell_1}} - \frac{1}{e^{a_1\ell_1} - e^{-a_1\ell_1}}\cdot\frac{X}{H}$$

$$D_1 = -\frac{H_p}{H}\cdot\frac{8f_1}{a_1^2\ell_1^2}\cdot\frac{e^{a_1\ell_1} - 1}{e^{a_1\ell_1} - e^{-a_1\ell_1}} + \frac{1}{e^{a_1\ell_1} - e^{-a_1\ell_1}}\cdot\frac{X}{H}$$

From the compatibility condition

$$\eta_1'(\ell_1) = \eta'(0)$$

we deduce the value of X

$$X = \frac{A_1a_1e^{a_1\ell_1} - A_3a_1e^{-a_1\ell_1} - B_1a + B_3a - \frac{H_p}{H}\left(\frac{4f}{\ell} + \frac{4f_1}{\ell_1}\right)}{\frac{1}{H\ell_1} - A_2a_1(e^{a_1\ell_1} + e^{-a_1\ell_1}) + B_2a - B_4a}$$

the constants A_i and B_i having the following expressions:

$$A_1 = \frac{H_p}{H}\cdot\frac{8f_1}{a_1^2\ell_1^2}\cdot\frac{1 - e^{-a_1\ell_1}}{e^{a_1\ell_1} - e^{-a_1\ell_1}} \qquad A_2 = \frac{1}{H}\frac{1}{e^{a_1\ell_1} - e^{-a_1\ell_1}}$$

$$A_3 = \frac{H_p}{H}\cdot\frac{8f_1}{a_1^2\ell_1^2}\cdot\frac{e^{-a_1\ell_1} - 1}{e^{a_1\ell_1} - e^{-a_1\ell_1}}$$

$$B_1 = \frac{H_p}{H}\cdot\frac{8f}{a^2\ell^2}\cdot\frac{1 - e^{-a\ell}}{e^{a\ell} - e^{-a\ell}} \qquad B_2 = \frac{1}{H}\frac{1 - e^{-a\ell}}{e^{a\ell} - e^{-a\ell}}$$

$$B_3 = \frac{H_p}{H}\cdot\frac{8f}{a^2\ell^2}\cdot\frac{e^{a\ell} - 1}{e^{a\ell} - e^{-a\ell}} \qquad B_4 = \frac{1}{H}\frac{e^{-a\ell} - 1}{e^{a\ell} - e^{-a\ell}}$$

The displacement δ can be evaluated by means of the Principle of Virtual Work. Assume the system in Fig. 3(b) as displacement system and that of Fig. 10 as force system. For the force system it is:

$$N = 1/\cos\alpha \quad M = -y$$

$$N_1 = 1/\cos\alpha_1 \quad M_1 = -y_1$$

in main and side span respectively. In the displacement system the cable tension due to the transversal loads is:

$$N = H_p/\cos\alpha$$

while the bending moment is, respectively in the main and side spans:

$$M(z) = -H\eta - H_p y + X$$

$$M_1(z_1) = -H\eta_1 - H_p\bar{y_1} + \frac{X}{\ell_1}z_1$$

The Principle of Virtual Work produces in this case:

$$\delta = \frac{H_a}{EA}L_s + 2\frac{H}{EI_1}\int_0^{\ell_1}\bar{y_1}\eta_1 dz + \frac{H}{EI}\int_0^{\ell}y\eta dz$$

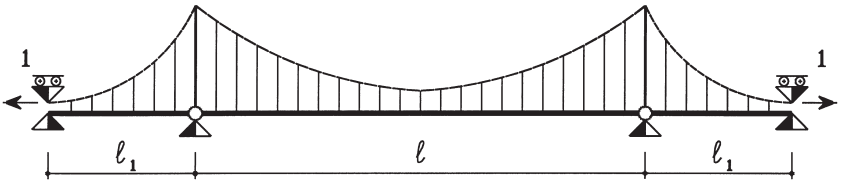

Fig. 10. Force system to calculate displacement δ by means of the Betti theorem.

$$+\frac{16}{15}\left(\frac{f_1^2\ell_1}{EI_1}+\frac{f^2\ell}{2EI}\right)H_p-\frac{2}{3}\left[\frac{f_1\ell_1}{EI_1}+\frac{f\ell}{EI}\right]X$$

where:

$$L_s=\int_A^B(1+y'^2)^{3/2}dz\cong 2\cdot\ell_1\frac{1}{\cos^3\alpha_1}\left(1+8\frac{f_1^2}{\ell_1^2}\right)+\ell\left(1+8\frac{f^2}{\ell^2}\right)$$

References

[1] Pugsley A. The theory of suspension bridges, 2nd ed. London: Arnold Ltd, 1968.

[2] Buonopane SG, Billington DP. Theory and history of suspension bridge design from 1923 to 1940. J Struct Engng ASCE 1993;119(3):954–77.

[3] Lin TY, Chow P. Gibraltar Strait crossing—a challenge to bridge and structural engineers. Struct Engng Int J IABSE 1991;1(2):53–8.

[4] Ulstrup CC. Rating and preliminary analysis of suspension bridges. J Struct Engng ASCE 1993;119(9):2653–79.

[5] Franciosi V. Lezioni di ponti. Napoli: Pellerano Del Gaudio, 1956.

[6] Nicolosi G, Raithel A, Clemente P. Static issues in very long-span suspension bridge design. In: Proceedings of the IABSE Symposium on Long-span and High-rise Structures. Zurich: IABSE, 1998:545–6.